PHYSICAL REVIEW B **92**, 241411(R) (2015)

Measurement of electronic heat dissipation in highly disordered graphene

N. Hemsworth,[1] F. Mahvash,[1,2] P. L. Lévesque,[3] M. Siaj,[2] R. Martel,[3] and T. Szkopek[1,*]

[1]*Department of Electrical and Computer Engineering, McGill University, Montréal, Québec, Canada H3A 2A7*

[2]*Department of Chemistry, Université du Québec à Montréal, Montréal, Québec, Canada H3C 3P8*

[3]*Department of Chemistry, Université de Montréal, Montréal, Québec, Canada H3C 3J7*

(Received 23 September 2015; published 28 December 2015)

We have measured the electronic heat dissipation of hot electrons in highly disordered millimeter scale graphene at temperatures $T = 0.3$–3 K. Disorder was introduced by hydrogenation of graphene, bringing low-temperature electron conduction below the Ioffe-Regel criterion for metallic conduction. Resistive thermometry was employed to determine the dependence of electron temperature on applied electrical power. The relation between heat flow and electron temperature was found to be well described by a power law with an exponent $\beta \sim 3.7$–3.9 and a coupling coefficient $\Sigma \sim 1\ \mathrm{mW/m^2\,K^\beta}$. Our observations are similar to electronic heat dissipation of a two-dimensional electron gas in the hydrodynamic limit of electron-phonon coupling, corresponding to acoustic phonon emission into the substrate.

DOI: 10.1103/PhysRevB.92.241411 PACS number(s): 65.80.Ck

Thermal transport in graphene has received much attention [1,2], motivated by fundamental questions into the nature of thermal transport in a semimetallic two-dimensional crystal. A variety of phenomena are experimentally observed, including thermal transport dominated by phonon transport [3–7], electron transport [8–11], and electron-phonon coupling [8,9,12–16]. Weak electron-phonon coupling at cryogenic temperatures enables the electron temperature to be easily driven in excess of lattice temperature, ideal for applications to hot electron bolometry. The heat flow from electrons to acoustic phonons is generally described by a power law, $\dot{Q} = A\Sigma(T_e^\beta - T_s^\beta)$, where A is the graphene area, Σ is the coupling constant, T_e is the electron temperature, T_s is the lattice temperature, and β is an exponent that characterizes the coupling. The electron-phonon coupling law is in general dependent upon the dimensionality, carrier density, temperature regime, screening, and disorder [17–20].

Theoretical work has shown that $\beta = 4$ for electron coupling to in-plane transverse acoustic (TA) and in-plane longitudinal acoustic (LA) phonons in pristine graphene at low temperatures [19,20]. Weakly disordered graphene with $k_F\ell \gg 1$, where k_F is the Fermi wave vector and ℓ the electron mean free path, admits the possibility of $\beta = 3$–6 [21]. An enhanced electron-phonon coupling assisted by defects with $\beta = 3$ and denoted supercollision cooling was predicted [22] at electron temperatures T_e exceeding the Bloch-Grüneisen temperature $T_{\mathrm{BG}} = 2\hbar c k_F / k_B$, where c is the acoustic velocity. Experiments with graphene monolayers have resulted in the observation of $\beta = 3$ and 4, including a transition $\beta = 4 \rightarrow 3$ consistent with the supercollision cooling mechanism [13]. A transition $\beta = 3 \rightarrow 4$ has also been observed in weakly disordered graphene as carrier density is tuned from the extrinsic regime to the intrinsic regime near charge neutrality [9], which remains as yet unexplained by theory. An enhancement in electron-phonon coupling with increasing disorder consistent with the supercollision mechanism has been observed in room temperature pump-probe transient absorption measurements [23]. Recently, electron-phonon coupling measured at $T < T_{\mathrm{BG}}$ was found to be suppressed in graphene disordered by plasma treatment [15], in contradiction with the supercooling mechanism.

In this Rapid Communication, we consider heavily disordered graphene, deep in the intrinsic, insulating regime that lies beyond the Ioffe-Regel criterion for metallic conductivity, $k_F\ell < 1$. By purposeful introduction of neutral point defects via hydrogenation, we have probed thermal transport in graphene deep in the insulating regime where $\partial R/\partial T < 0$. Qualitative agreement with variable range hopping (VRH) is observed in the electron transport of graphene with disorder induced by hydrogenation [24,25]. The resistance of disordered graphene exhibits strongly insulating behavior $\partial R/\partial T < 0$, enabling simple resistive thermometry of electron temperature as commonly employed in disordered systems [26–28].

We investigated electron heating in three devices: two hydrogenated devices (HG1 and HG5), and one pristine device (G3). All three devices were prepared from graphene grown by chemical vapor deposition (CVD) and transferred to silicon substrates with a 300 nm layer of dry thermal oxide. The devices were electrically contacted with indium, requiring no lithography and thereby minimizing the possibility for undesired reaction between resists and hydrogenated graphene. Indium's superconducting state at $T < 3.4$ K also aids in suppressing electronic heat conduction through the electrical contacts. Hydrogenation was performed in an ultrahigh vacuum environment at room temperature with an atomic hydrogen beam, as reported in previous work [25,29]. Exposure times were between 3 and 10 min with both HG1 and HG5 having exposure times of 5 min.

To characterize the degree of hydrogenation, specifically the density of defects breaking the translational symmetry of the ideal honeycomb lattice of sp^2 hybridized carbon, Raman spectroscopy was performed with a pump wavelength of $\lambda = 532$ nm. The ratio of the Raman D-band ($1345\ \mathrm{cm^{-1}}$) intensity I_D to the Raman G-peak ($1585\ \mathrm{cm^{-1}}$) intensity I_G was used to estimate defect density, along with the Raman D' band ($1626\ \mathrm{cm^{-1}}$), relying upon a calibration determined from Ar-ion bombardment of graphene [30]. The properties of HG1, G3, and HG5 are summarized in Table I.

*thomas.szkopek@mcgill.ca

TABLE I. The measured samples are summarized below, including effective graphene channel length L and width W between contacts, low-bias two-point resistance R_{2pt} at $T = 300$ mK, and Raman Stokes peak intensity ratio I_D/I_G. The mean defect spacing L_D inferred from Raman analysis is also included.

Device	$L \times W$ (mm)	R_{2pt} (kΩ)	I_D/I_G	L_d (nm)
HG1	2.28×1.3	53	2.4 ± 0.15	5.5 ± 0.5
G3	2.48×1.9	8.9	0.40 ± 0.11	17 ± 2
HG5	2.27×1.5	720	2.1 ± 0.65	1.7 ± 0.3

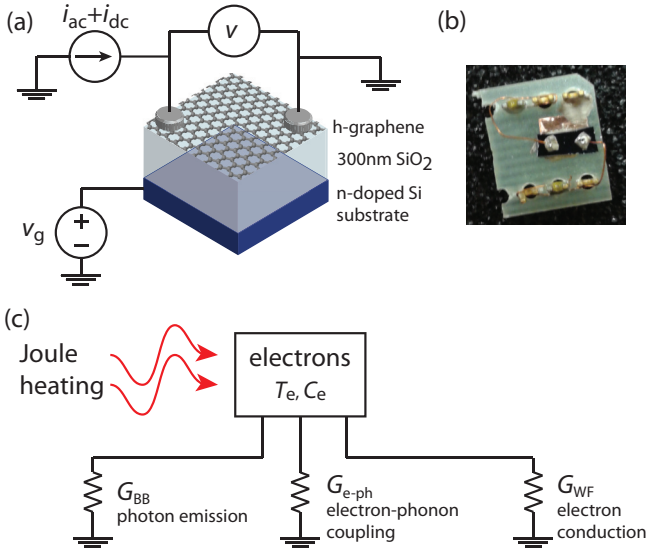

FIG. 1. (Color online) (a) Schematic of the experimental setup used to perform electrical measurements. (b) Optical micrograph of sample HG1. (c) Schematic of a thermal model describing the Joule heating of electrons and heat flow through three distinct channels: blackbody photon emission, electron-phonon coupling, and electron conduction.

Electron and thermal transport measurements were performed under high vacuum conditions in a He^3 cryostat. The silicon substrate was thermally anchored to metal pins on a fiberglass (G10) header using a conductive epoxy. The wiring for both the silicon substrate and the graphene contacts was wrapped tightly around a gold-plated bobbin that was thermally anchored to the He^3 pot. This ensured a strong thermal link between the He^3 pot and the substrate. The sample lattice temperature T_s was tuned between 300 mK and 3 K under high vacuum conditions. The differential electrical resistance $R = v_{ac}/i_{ac}$ was measured in a two-point configuration as illustrated in Fig. 1 using a lock-in amplifier operating at $f = 11.438$ Hz. A superimposed dc source was used to directly heat the hydrogenated graphene with $\dot{Q} = < iv >$ total electrical bias power while the differential resistance was simultaneously measured. The back-gate potential v_g was varied to modulate the conductivity of the hydrogenated graphene.

The two-point differential resistance R was used as an internal thermometer of the graphene electron temperature T_e, explained in greater detail below. A simple thermal model incorporating three thermal channels, illustrated in Fig. 1(c), was adopted to interpret our experimental results. Blackbody photon emission $\dot{Q}_{BB} = A\sigma(T_e^4 - T_s^4)$ to the cold environment of the sample is found to be negligible in our experiments because the Stefan-Boltzmann constant $\sigma = 56.7\ \mathrm{nW\,m^{-2}\,K^{-4}}$ is much smaller than our experimentally measured electron-phonon coupling constant Σ. Thermal conductance G_{WF} by electronic conduction is also found to be negligible by theoretical estimations. Considering an electrical sheet resistance of order $r \approx 100$ kΩ typical of our experiments, the thermal sheet conductance can be estimated coarsely by a Wiedemann-Franz relation $g_{WF} = r^{-1}L_0T_e = 245\ \mathrm{fW\,K^{-1}}$ at an electron temperature $T_e = 1$ K and free electron Lorenz number $L_0 = 24.5\ \mathrm{nW\,\Omega\,K^{-2}}$. Taking into account a graphene width/length ratio $W/L \approx 0.5$, and a model one-dimensional temperature profile along the graphene length [10], the thermal conductance by electron conduction $G_{WF} = 12(W/L)g_{WF} \approx 1.4\ \mathrm{pW\,K^{-1}}$, which is of negligible magnitude compared to that experimentally observed. We conclude that thermal conductance $G_{e\text{-ph}}$ via electron-phonon coupling is the dominant channel for thermal conduction.

The measured differential resistance R versus electrical bias power $\dot{Q}$ with substrate temperature T_s as a parameter is plotted in Fig. 2(a) for sample HG5. A plateau in resistance R defines the low-bias region where Joule heat causes a negligible resistance change and $T_e = T_s$. The differential resistance is observed to decrease with increasing electrical bias power, $T_e > T_s$, and is also observed to decrease with increasing substrate temperature as expected of an insulator ($\partial R/\partial T < 0$). The resistance is also observed to increase with increasing back-gate voltage, $\partial R/\partial V_g > 0$, consistent with hole hopping conduction as observed in previous experiments with graphene hydrogenated on an oxide surface [25]. In both strongly disordered samples HG1 and HG5 where $k_F\ell < 1$, the charge neutrality point was beyond our experimentally accessible gate voltage range. In the weakly disordered sample, G3, the charge neutrality point was estimated by fitting the measured low-bias resistance R versus gate voltage V_g to a simple diffusive conductivity model $1/R \propto p$ with hole density $p = C(V_g - V_{CNP})$, where $C = 11.5\ \mathrm{nF\ cm^{-2}}$. The charge neutrality point was determined to be $V_{CNP} = +71$ V, corresponding to a mobile hole density $p_0 = 3 \times 10^{12}\ \mathrm{cm^{-2}}$ at $V_g = 0$ V.

The low-bias resistance R is plotted versus substrate temperature T_s in Fig. 2(b), along with an empirical best-fit curve to establish a resistive thermometer calibration. The coefficient of determination for all resistive calibrations was >99%. Resistive thermometry is often used to infer mean electron temperature in insulating thin films with strong temperature dependent resistance [26–28]. In addition to Joule heating of electrons, electric field dependent transport may contribute an additional variation of differential resistance versus electrical bias [31]. An applied electric field $\mathcal{E}$ will produce negligible excess current as compared to thermal excitation when $e\mathcal{E}a \ll k_BT_e$, where a is a characteristic length scale of the carrier confinement potential. At the lowest temperature $T_e = 300$ mK and highest field $\mathcal{E} = 100\ \mu\mathrm{V}/\mu\mathrm{m}$

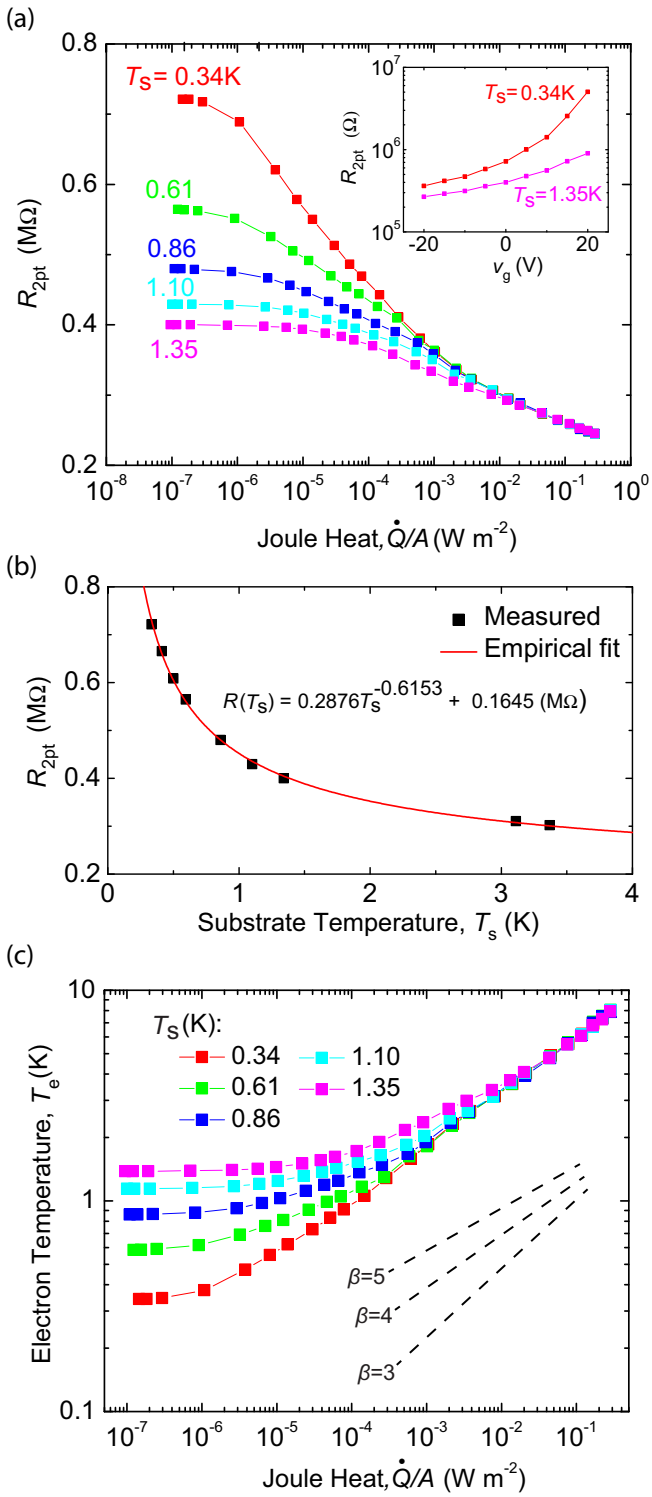

FIG. 2. (Color online) (a) The differential two-point resistance R_{2pt} vs the electrically applied Joule heating power per unit area $\dot{Q}/A$ for sample HG5 at a substrate temperature $T_s = 0.34$ K. Low-bias plateaus are evident, as is a decrease in resistance with applied power. The inset shows the low-bias R_{2pt} vs gate voltage v_g at substrate temperatures $T_s = 0.34$ and 1.35 K. (b) The low-bias resistance R_{2pt} vs temperature $T_s = T_e$ for HG5, including measurements (squares) and empirical fit (line) used for resistive thermometry. (c) The inferred electron temperature T_e vs Joule heating $\dot{Q}/A$ at various substrate temperatures T_s. Slopes corresponding to $\dot{Q} \propto T_e^{\beta}$ with $\beta = 3,4,5$ are shown for comparative purposes.

applied in our experiments, electrons confined to traps with $a > 260$ nm will contribute excess current. By comparison, the mean hydrogenation induced defect spacing is $L_D = 2$–6 nm, corresponding to a much shorter length scale, suggesting field induced excess currents are negligible in our work.

The empirical fit function $R_0(T_s)$ of low-bias resistance versus temperature $T_e = T_s$ was thus used to infer an electron temperature T_e from the measured differential resistance R versus applied electrical bias power $\dot{Q}$, and is plotted in Fig. 2(c). At low bias, the electron temperature T_e is independent of applied power, while at high bias, the electron temperature follows an asymptotic $T_e \propto \dot{Q}^{1/4}$ dependence. Our observations are consistent with a heat dissipation law $\dot{Q} = A\Sigma(T_e^{\beta} - T_s^{\beta})$ with $\beta = 4$. The applied power $\dot{Q}$ versus temperature function $T_e^4 - T_s^4$ is plotted in Fig. 3 on logarithmic scales for samples HG1, HG5, and G3, indicating consistent behavior across orders of magnitude in applied heat $\dot{Q}$ and substrate temperature T_s. A least-squares fit of $\dot{Q}$ vs $T_e^{\beta} - T_s^{\beta}$ on a logarithmic scale gives $\beta = 3.66 \pm 0.05$ for HG1, $\beta = 3.82 \pm 0.16$ for HG5, and $\beta = 3.87 \pm 0.14$ for G3. Similarly, the coupling parameter $\Sigma = 1.3 \pm 0.1$ mW/m^2 K$^{\beta}$ for HG1, $\Sigma = 0.11 \pm 0.03$ mW/m^2 K$^{\beta}$ for HG5, and $\Sigma = 0.8 \pm 0.01$ mW/m^2 K$^{\beta}$ for G3.

We present in Fig. 4(a) a summary of experimentally measured β exponent versus normalized low-bias resistance $(2e^2/h)R_{2pt}$, which gives an approximation to the Ioffe-Regel disorder parameter $(k_F\ell)^{-1}$, for our work and previously reported work. Exponents $\beta = 4$ and 3 have both been previously reported at $T_e < T_{BG}$ for a variety of graphene devices [8,9,12,13], with a transition $\beta = 3 \rightarrow 4$ observed as the carrier density is tuned to charge neutrality and increased resistance [9]. In our work, $\beta \approx 4$ is observed for both weakly disordered pristine graphene and strongly disordered hydrogenated graphene over all ranges of gate voltage explored. The coupling constant Σ is similarly presented in Fig. 4(b) versus normalized low-bias resistance $(2e^2/h)R_{2pt}$, and is surprisingly found to be independent of the sample resistance (tuned by back gate voltage). As seen in Fig. 4, our measured $\Sigma \sim 0.1$–1 mW/m^2 K$^{\beta}$ is of comparable value to that reported for exfoliated graphene on BN/SiO_2/Si and CVD graphene on SiO_2/Si where $\beta = 4$ was also observed [12], and the small coupling constant was explained as potentially arising from lattice disorder.

There is presently no theory for electron energy loss in graphene in the strongly disordered limit $(k_F\ell)^{-1} \gg 1$ with which to compare our experimental observations. The supercollision mechanism observed in weakly disordered graphene [13,14], characterized by $\beta = 3$, was not observed in our samples. However, experiments conducted with two-dimensional electron gases (2DEGs) in GaAs/$AlGa_{1-x}As$ heterostructures have revealed a $\beta = 4$ law for electron-phonon coupling [27,32,33], in accordance with the theory of electron-phonon coupling in a piezoelectric medium in the hydrodynamic limit where the electron-impurity scattering rate exceeds the electron-phonon scattering rate [32]. In the hydrodynamic limit, relaxation of momentum conservation in the electron-phonon scattering process enables the 2DEG to emit acoustic phonons directly into the bulk substrate and superstrate, with a $\dot{Q} \propto T_e^4$ dependence reminiscent of

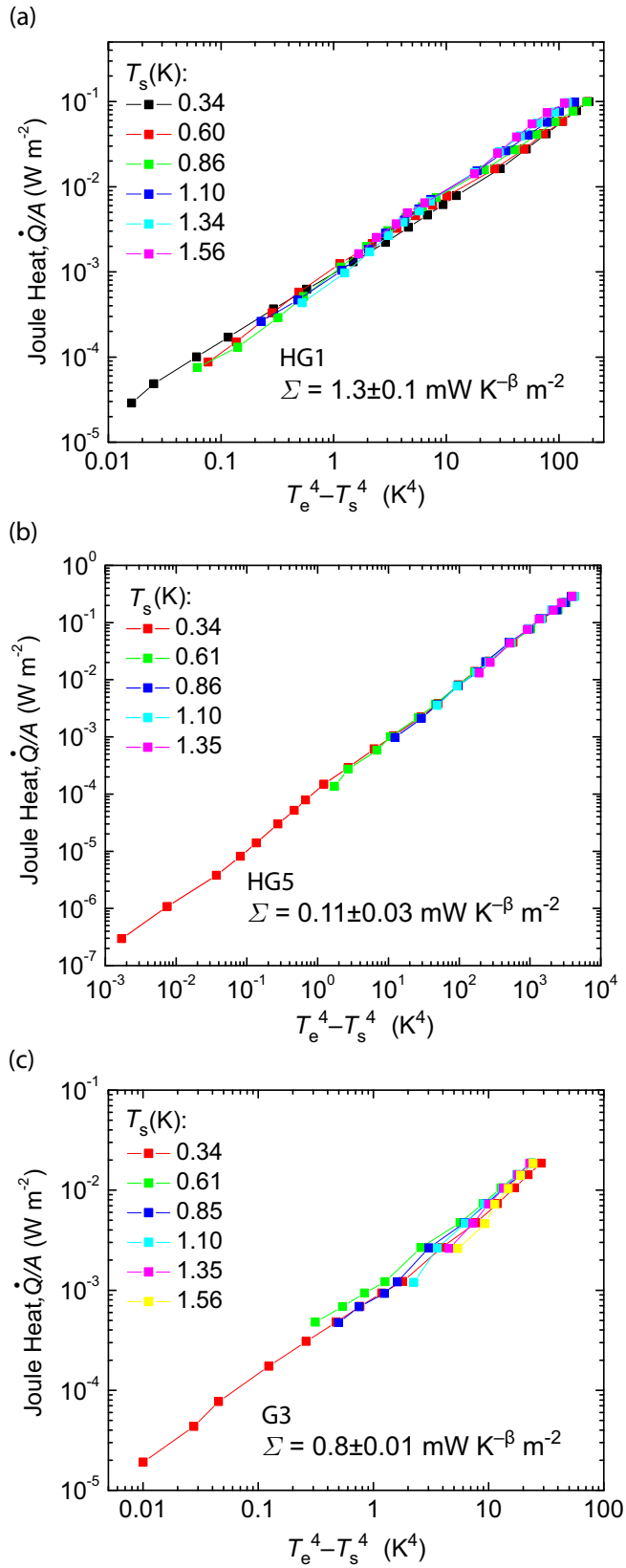

FIG. 3. (Color online) The Joule heating power per unit area $\dot{Q}/A$ vs temperature parameter $T_e^4 - T_s^4$ for hydrogenated graphene samples (a) HG1, (b) HG5, and pristine graphene sample (c) G3. The coupling parameter Σ inferred from a least-squares fit is indicated for each sample, respectively.

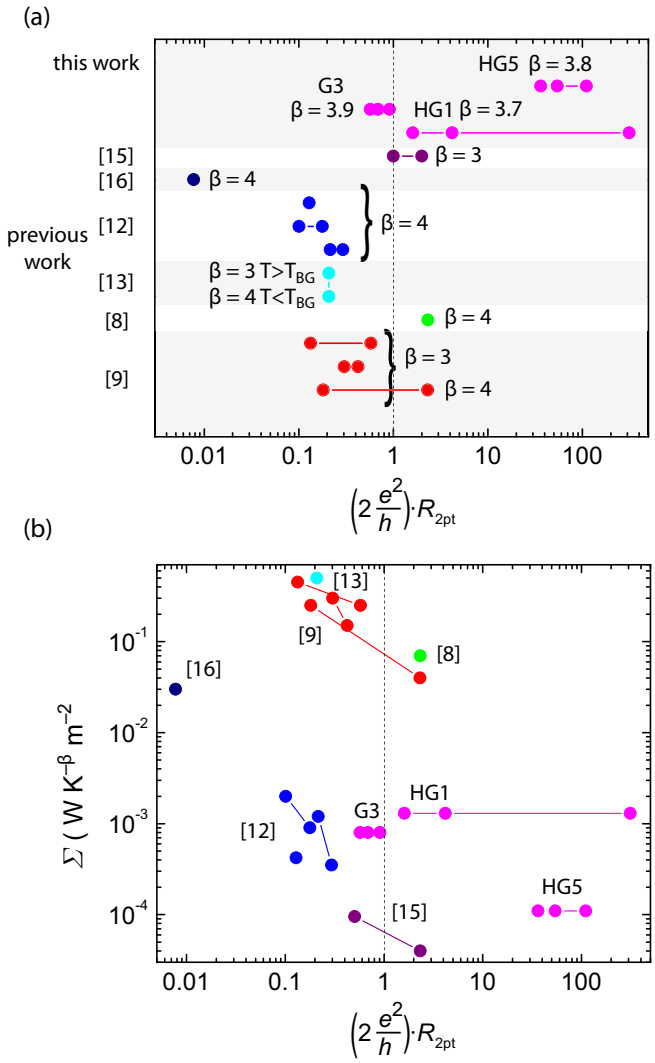

FIG. 4. (Color online) (a) A summary of the β exponent vs the normalized low-bias two-point resistance $2e^2/hR_{2pt}$ measured for samples HG1, HG5, and G3, and previous reports of electron-phonon coupling in monolayer graphene [8,9,12,13,15,16]. (b) A summary of the coupling strength Σ vs $2e^2/hR_{2pt}$ for samples HG1, HG5, and G3, and previous reports.

a Stefan-Boltzmann law $\dot{Q} = A\sigma T^4$ and a typical thermal boundary resistance giving $\dot{Q} = A\Sigma' T^4$ [34]. A similar scenario may apply to strongly disordered graphene supported by a substrate, wherein point defects in the graphene lattice may play a role in the coupling amongst electrons, in-plane LA and TA graphene phonons, out-of-plane acoustic (ZA) graphene phonons, and SiO_2 phonons. Unravelling the microscopic details of energy transfer requires further experimental work.

In conclusion, we have observed electronic heat dissipation following a $\dot{Q} = A\Sigma(T_e^\beta - T_s^\beta)$ law with exponent $\beta = 3.7$–3.9 and coupling coefficient $\Sigma \sim 0.1$–1 mW/m^2 K$^\beta$ for pristine CVD graphene and hydrogenated CVD graphene in the strongly disordered limit where $(k_F\ell)^{-1} \gg 1$. There is a need to extend the theory of electron-phonon coupling in weakly disordered graphene [21,22] to the strongly disordered limit. Our observations are similar to previously reported

measurements of hot electron energy loss in weakly disordered graphene exfoliated on $BN/SiO_2/Si$ [12], and are also similar to hot electron energy loss of 2DEGs in the hydrodynamic limit of $GaAs/AlGa_{1-x}As$ heterostructures.

The authors thank the Natural Sciences and Engineering Research Council of Canada, Canada Research Chairs program, and the Fonds du Recherche Québécois–Natures et Technologies for financial support of this work.

[1] A. A. Balandin, Thermal properties of graphene and nanostructured carbon materials, Nat. Mater. **10**, 569 (2011).

[2] E. Pop, V. Varsheny, and A. K. Roy, Thermal properties of graphene: fundamentals and applications, MRS Bull. **37**, 1273 (2012).

[3] A. A. Balandin *et al.*, Superior thermal conductivity of single layer graphene, Nano Lett. **8**, 902 (2008).

[4] S. Ghosh *et al.*, Extremely high thermal conductivity in graphene: Prospects for thermal management application in nanoelectronic circuits, Appl. Phys. Lett. **92**, 151911 (2008).

[5] W. Cai *et al.*, Thermal transport in suspended and supported monolayer graphene grown by chemical vapor deposition, Nano Lett. **10**, 1645 (2010).

[6] C. Faugeras *et al.*, Thermal conductivity of graphene in Corbino membrane geometry, ACS Nano **4**, 1889 (2010).

[7] J. H. Seol *et al.*, Two-dimensional phonon transport in supported graphene, Science **328**, 213 (2010).

[8] K. C. Fong and. K. C. Schwab, Ultrasensitive and Wide-Bandwidth Thermal Measurements of Graphene at Low Temperatures, Phys. Rev. X **2**, 031006 (2012).

[9] K. C. Fong, E. E. Wollman, H. Ravi, W. Chen, A. A. Clerk, M. D. Shaw, H. G. Leduc, and K. C. Schwab, Measurement of the Electronic Thermal Conductance Channels and Heat Capacity of Graphene at Low Temperature, Phys. Rev. X **3**, 041008 (2013).

[10] S. Yigen, V. Tayari, J. O. Island, J. M. Porter, and A. R. Champagne, Electronic thermal conductivity measurements in intrinsic graphene, Phys. Rev. B **87**, 241411(R) (2013).

[11] S. Yigen and A. R. Champagne, Wiedemann-Franz relation and thermal-transistor effect in suspended graphene, Nano Lett. **14**, 289 (2014).

[12] A. C. Betz *et al.*, Hot Electron Cooling by Acoustic Phonons in Graphene, Phys. Rev. Lett. **109**, 056805 (2012).

[13] A. C. Betz *et al.*, Supercollision cooling in undoped graphene, Nat. Phys. **9**, 109 (2013).

[14] M. W. Graham *et al.*, Photocurrent measurements of supercollision cooling in graphene, Nat. Phys. **9**, 103 (2013).

[15] Q. Han, Y. Chen, G. Liu, D. Yu, and X. Wu, Observation of vacancy-induced suppression of electronic cooling in defected graphene, Phys. Rev. B **91**, 121404(R) (2015).

[16] C. B. McKitterick *et al.*, Ultrasensitive graphene far-infrared power detectors, J. Phys.: Condens. Matter **27**, 164203 (2015).

[17] R. Bistritzer and A. H. MacDonald, Electronic Cooling in Graphene, Phys. Rev. Lett. **102**, 206410 (2009).

[18] W.-K. Tse and S. Das Sarma, Energy relaxation of hot Dirac fermions in graphene, Phys. Rev. B **79**, 235406 (2009).

[19] S. S. Kubakaddi, Interaction of massless Dirac electrons with acoustic phonons in graphene at low temperatures, Phys. Rev. B **79**, 075417 (2009).

[20] J. K. Viljas and T. T. Heikkilä, Electron-phonon heat transfer in monolayer and bilayer graphene, Phys. Rev. B **81**, 245404 (2010).

[21] W. Chen and A. A. Clerk, Electron-phonon mediated heat flow in disordered graphene, Phys. Rev. B **86**, 125443 (2012).

[22] J. C. W. Song, M. Y. Reizer, and L. S. Levitov, Supercollisions and the Bottleneck for Electron-Lattice Cooling in Graphene, Phys. Rev. Lett. **109**, 106602 (2012).

[23] T. V. Alencar *et al.*, Defect-induced supercollision cooling of photoexcited carriers in graphene, Nano Lett. **14**, 5621 (2014).

[24] D. C. Elias *et al.*, Control of graphene's properties by reversible hydrogenation: evidence for graphane, Science **323**, 610 (2009).

[25] J. Guillemette *et al.*, Quantum Hall Effect in Hydrogenated Graphene, Phys. Rev. Lett. **110**, 176801 (2013).

[26] S. Marnieros, L. Bergé, A. Juillard, and L. Dumoulin, Dynamical Properties Near the Metal-Insulator Transition: Evidence For Electron-Assisted Variable Range Hopping, Phys. Rev. Lett. **84**, 2469 (2000).

[27] E. Chow, H. P. Wei, S. M. Girvin, W. Jan, and J. E. Cunningham, Effect of disorder on phonon emissions from a two-dimensional electron gas in $GaAs/Al_xGa_{1-x}As$ heterostructures, Phys. Rev. B **56**, R1676(R) (1997).

[28] M. Galeazzi *et al.*, Hot-electron effects in strongly localized doped silicon at low temperature, Phys. Rev. B **76**, 155207 (2007).

[29] K. Bennaceur *et al.*, Measurement of topological Berry phase in highly disordered graphene, Phys. Rev. B **92**, 125410 (2015).

[30] M. M. Lucchese *et al.*, Quantifying ion-induced defects and Raman relaxation length in graphene, Carbon **48**, 1592 (2010).

[31] T. Kenny, P. L. Richards, I. S. Park, E. E. Haller, and J. W. Beeman, Bias-induced nonlinearities in the dc *I-V* characteristics of neutron-transmutation-doped germanium at liquid-^{4}He temperatures, Phys. Rev. B **39**, 8476 (1989).

[32] E. Chow, H. P. Wei, S. M. Girvin, and M. Shayehan, Phonon Emission from a 2D Electron Gas: Evidence of Transition to the Hydrodynamic Regime, Phys. Rev. Lett. **77**, 1143 (1996).

[33] R. Fletcher, Y. Feng, C. T. Foxon, and J. J. Harris, Electron-phonon interaction in a very low mobility $GaAs/Ga_xAl_{1-x}As$ δ-doped gated quantum well, Phys. Rev. B **61**, 2028 (2000).

[34] F. Pobell, *Matter and Methods at Low Temperatures*, 3rd ed. (Springer, Berlin, 2007).